eprints@whiterose.ac.uk
https://eprints.whiterose.ac.uk/

Influence of Conduction Angles on Single Layer Switched Reluctance Machines

G. J. Li, Member, IEEE, X. Y. Ma, G. W. Jewell, Z. Q. Zhu, Fellow, IEEE, and P. L. Xu

University of Sheffield, Sheffield, S1 3JD, U.K.

g.li@sheffield.ac.uk

Abstract—**This paper investigates the influence of conduction angles on the performances of two 3-phase 12-slot/8-pole short pitched switched reluctance machines (SRMs): single layer SRM with conventional winding (SL-CSRM), and single layer SRM with mutually coupled winding (SL-MCSRM). Both unipolar and bipolar excitations are employed for the SRMs with different conduction angles such as unipolar 120° elec., unipolar 180° elec., bipolar 180° elec., bipolar 240° elec., and bipolar 360° elec. Their flux distributions, self- and mutual-flux linkages and inductances are analyzed, and followed by a performance comparison in terms of on-load torque, average torque, torque ripple, using two-dimensional finite element method (2D FEM). Copper loss, iron loss and machine efficiency have also been investigated with different phase currents and rotor speeds. The predicted results show that the conduction angle of unipolar 120° elec. is the best excitation approach for SL-CSRM at low current and also modest speed, as its double layer counterpart. However, at high current, the higher average torque is achieved by a conduction angle of unipolar 180° elec. For SL-MCSRM, bipolar 180° elec. conduction is the most appropriate excitation method to generate a higher average torque but lower torque ripple than others. The lower iron loss is achieved by unipolar excitation, and the SLCSRM with unipolar 120° elec. conduction produces the highest efficiency than others at $10A_{rms}$. In addition, the performances of single layer machines have been compared with the established double layer SRMs with conventional and mutually-coupled windings. The prototype SRMs, for both SL-CSRM and SL-MCSRM, have been built and tested to validate the predictions.**

Keywords—**bipolar excitation, single layer, switched reluctance machine, unipolar excitation.**

I. INTRODUCTION

ELECTRICAL machines have been employed in many applications, ranging from automotive, wind turbine, aerospace, robotics, and domestic appliances, etc. [1] [2]. The literature review has revealed that about 40% of electrical machines [induction machine, permanent magnet machine, switched reluctance machine (SRM)] are used for automotive applications and the SRMs are attracting increasing interest owning to the merits such as no permanent magnets and hence low cost, simple and robust rotor structure [2] [3]. However, due to its doubly salient structure, the SRMs inherently exhibit high torque ripple, high acoustic noise and vibrations [4].

In order to minimize the torque ripple, several reduction strategies have been proposed such as modifying stator and rotor pole geometry [5] - [6], employing high rotor pole numbers [7], and profiling the current waveforms [8] [9]. Generally, SRMs are supplied by unipolar current using an asymmetric bridge inverter, and the conduction angle of phase current for conventional SRMs is ≤120° elec. without any phase overlapping. In order to extend the overlap time during the commutation for torque ripple reduction, bipolar excitation is applied to SRMs and a three-phase H-bridge inverter needs to be employed [10] [11].

Two bipolar excitations have been investigated in literature, i.e. rectangular and sinusoidal waveforms. In [12], two phases of SRM are excited simultaneously. Hence, the torque is produced by both self- and mutual-inductances. Moreover, mechanical stress can be mitigated due to the reduced abrupt change of phase excitation. Similarly, indicated by this hybrid excitation, the vibration and acoustic noise are reduced [13]. It has also been found that with sinusoidal bipolar excitation, torque ripple of double layer conventional SRM (DL-CSRM) can be reduced when compared to unipolar excitation and bipolar excitation with rectangular waveforms [14]. In addition, the double layer mutually coupled SRM (DL-MCSRM) with sinusoidal

bipolar excitation produced higher average torque but lower torque ripple than that supplied by rectangular waveforms current [15]. However, average torque of DL-CSRM is often lower than that of DL-MCSRM due to the nature of self- and mutual-inductances [16]. In order to further improve the torque capability, fully-pitched SRMs (FPSRMs) with single layer winding structure have been proposed [17]. They have much higher position varying mutual-inductance and can produce high average torque but low torque ripple [16] [17] [18]. However, the longer end-winding will lead to higher copper loss, limiting their efficiency.

Two novel short pitched, single layer (SL-) SRMs proposed in [16] [19] have combined the merits of single layer FPSRM and short-pitched DL-CSRM/DL-MCSRM, in which the phase currents are sinusoidal. However, due to the different waveforms of the derivatives of self- and mutual- inductances with respect to rotor positions, the current waveforms can be tailored accordingly in order to improve the torque performance. In this paper, the SL-SRMs will be supplied by unipolar and bipolar excitations with rectangular waveforms and variable conduction angles such as unipolar 120° elec., unipolar and bipolar 180° elec., bipolar 240° elec. and bipolar 360° elec. will be employed. Hence, the contribution of this paper is to comprehensively investigate two novel single layer SRMs supplied by different unipolar and bipolar excitations. The influence of conduction angles on the machine performance is studied and compared in terms of instantaneous torque, average torque and torque ripple at both low current and high current levels. Furthermore, after the calculation of copper loss and iron loss, the machine efficiency has been investigated under different speeds and currents. Based on the obtained results, the appropriate excitation method can be found for different machines in order to achieve higher torque, lower torque ripple and also higher efficiency under different conditions.

In this paper, features of two SRMs, i.e. SL-CSRM and SL-MCSRM are introduced in terms of winding configuration, self- and mutual flux linkages, and self- and

mutual-inductances and their derivatives in Section II. Different current waveforms with different conduction angles are selected according to the inductance waveforms in order to achieve better torque performance in Section III. The influence of different conduction angles on machine performance such as electromagnetic torque, copper and iron losses and also efficiency of the SL-SRMs is investigated by 2-D finite element method (2-D FEM) in Section IV. Experiments are carried out to validate the predicted results in Section V. Section VI gives general conclusions.

II. FEATURES OF SL-SRMs

A. Features of Two SL-SRMs

In this paper, all the machines have the same dimensions and design parameters as summarized in TABLE I. The winding configurations of the two 3-phase, 12-slot/8-pole SL-SRMs are based on the established DL-CSRM and DL-MCSRM as shown in Fig. 1(a) and Fig. 1 (b). Fig. 1 (c) and Fig. 1 (d) show the SL-CSRM and SL-MCSRM, respectively [19]. The rotors of the SRMs are at the aligned position of phase A which supplied by a 10A dc current. It can be found that the number of exciting poles (number of coils of phase A) of DL-SRMs is doubled than that of the SL-SRMs. Hence, the magnetic paths in DL-SRMs are shorter than that in SL-SRMs, which indicate less sensitivity to magnetic saturation. In order to maintain the same number of turns per phase as for the established DL-SRMs, each coil of SL-SRMs has double number of turns since their number of coils has halved compared with the DL-SRMs. However, both SL- and DL-SRMs employ concentrated windings. Therefore, their end-windings are much shorter than the same sized FPSRM, leading to lower copper loss [19].

TABLE I. MACHINE LEADING DIMENSIONS AND DESIGN PARAMETERS

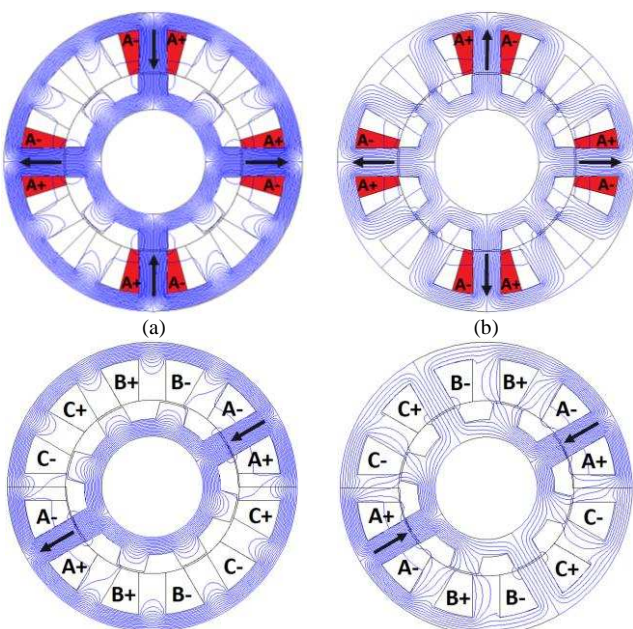| Parameter	Value	Parameter	Value
Stator slot number	12	Active length (mm)	60
Rotor pole number	8	Turn number per phase	132
Stator outer radius (mm)	45	Coil packing factor	0.37
Air gap length (mm)	0.5	Rated RMS current (A)	10
Rotor outer radius (mm)	26.5	Current density (A_{rms}/mm^2)	5.68
Rotor inner radius (mm)	15.7		

(a) (b)

Fig. 1. Comparison of winding configurations and flux distributions between (a) DL-CSRM, (b) DL-MCSRM (c) SL-CSRM and (d) SL-MCSRM. The rotor is at aligned position and phase A is supplied by a 10A dc current.

Similar to the established DL-CSRM, it is found that there exists almost no mutual flux in SL-CSRM, hence better fault tolerant capability [20]. However, due to different magnetic polarities in SL-MCSRM, the fluxes of phase A also link with phases B and C. Therefore, the mutual flux exists in the SL-MCSRM (similar to the DL-MCSRM) and will contribute to torque generation [6].

B. Self- and Mutual-Flux Linkages

Due to magnetic saturation, the flux linkage loci with increasing phase current are nonlinear. They are also determined by the rotor position due to the doubly salient structure. The maximum flux linkage is achieved at aligned position while the minimum occurs at unaligned position as shown in Fig. 2, where phase A is supplied by an increasing dc current. It can be found that SL-MCSRM can resist a higher saturation current than SL-CSRM since SL-MCSRM is less sensitive to magnetic saturation. Moreover, it is worth noting that since the SL-SRMs have doubled the number of turns per coil compared to DL-SRMs, leading to higher MMF concentration, they will be more prone to magnetic saturation than their DL counterparts.
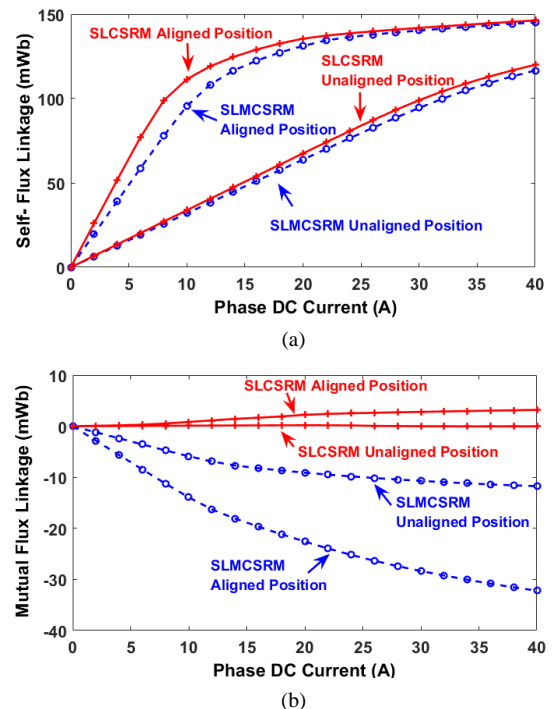

(a)

(b)

Fig. 2. Comparison of flux linkage of phase A against phase DC current of SL-CSRM and SL-MCSRM. (a) self-flux linkage. (b) mutual-flux linkage.

The area enclosed by the locus between aligned and unaligned positions is the co-energy (W'), which converts the electrical energy to mechanical energy of SRMs, or vice versa. According to the co-energy theory, the instantaneous torque T and average torque T_{av} can be given by [2] [21]:

$$T = \frac{\partial W'(i,\theta)}{\partial \theta}\bigg|_{i=constant} \tag{1}$$

$$T_{av} = \frac{mp}{2\pi} \times W' \tag{2}$$

where i is the instantaneous phase current, θ is the rotor position, m is number of phases, and p is pole pair numbers. Therefore, the torque produced by self-flux linkage (self-inductance) of SL-CSRM will be slightly higher than that of SL-MCSRM due to the bigger area enveloped by the aligned and unaligned self-flux linkages in Fig. 2 (a). However, the area enclosed by the aligned and unaligned mutual-flux linkages of SL-CSRM is significantly smaller than SL-MCSRM as shown in Fig. 2 (b). This means that the current waveforms will have significantly different influences on the performance of both SL-SRMs, as will be detailed in the following sections.

C. Self- and Mutual-Inductances

In order to employ the appropriate current waveforms for SL-SRMs, self- and mutual inductances have been analyzed separately. According to self- and mutual flux linkages, the apparent self-inductances L_a, L_b and L_c, and mutual-inductances M_{ab}, M_{bc}, and M_{ca} can be calculated by 2-D FEM respectively.

(1). Self-Inductance

Fig. 3 shows the comparison of self- and mutual-inductances of both SL-SRMs, and Fig. 4 shows the derivatives of self-inductance with respect to rotor position ($dL/d\theta$) from 2A to 20A dc current.
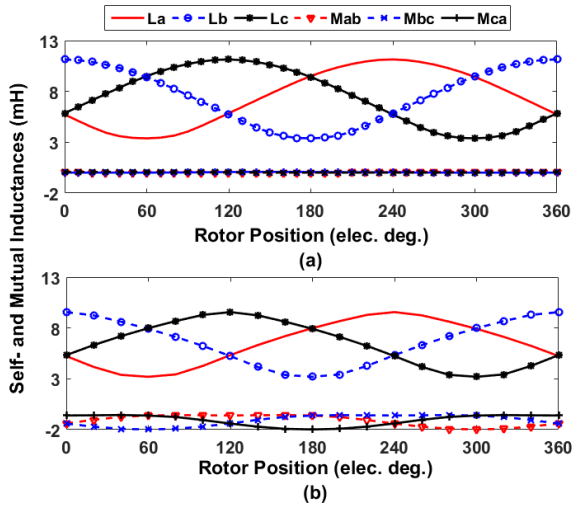
Fig. 3. Comparison of self- and mutual-inductances. (a) SL-CSRM, and (b) SL-MCSRM. Phases A, B and C are supplied by a 10A dc current, respectively.
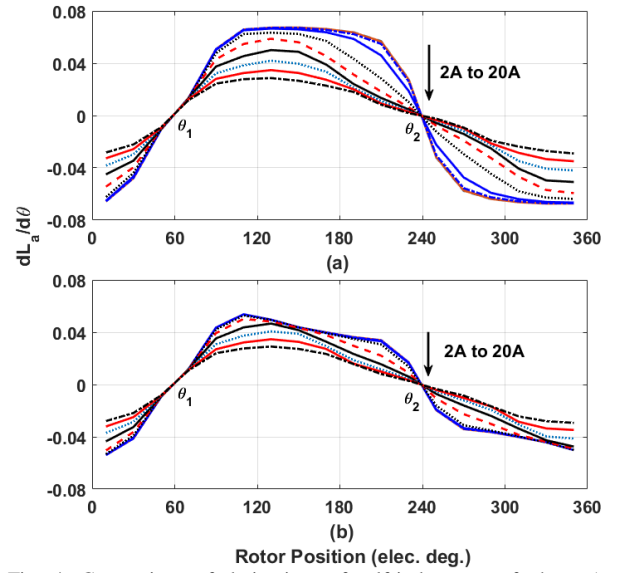
Fig. 4. Comparison of derivatives of self-inductance of phase A with respect to rotor position. (a) SL-CSRM and (b) SL-MCSRM. Phases A supplied by dc current from 2A to 20A.

It is found that the positive $dL/d\theta$ of both the SL-SRMs lasts for 180° elec. and the two rotor positions for $dL/d\theta = 0$ can be expressed as:

$$\begin{bmatrix} \theta_1 \\ \theta_2 \end{bmatrix} = \begin{bmatrix} (\pi/N_r - \alpha/2) \times N_r \\ (2\pi/N_r - \alpha/2) \times N_r \end{bmatrix} \quad (3)$$

where N_r is rotor pole number and α is angle between initial rotor position and rotor aligned position in mechanical degrees. However, the amplitude of $dL/d\theta$ of SL-CSRM is slightly higher than that of SL-MCSRM. Hence, the SL-CSRM is likely to produce higher self-torque (torque produced by self-inductance) [16]. However, it is worth noting that the electromagnetic torque can be produced by both the derivatives of self- and mutual-inductances with respect to rotor position, and also depends directly on the current waveforms.

(2). Mutual-Inductance

Different winding configurations lead to different flux paths in SL-SRMs. It has been found that mutual-inductances only exist in SL-MCSRM as shown in Fig. 3. Fig. 6 (a) shows the derivatives of mutual-inductance with respect to rotor position ($dM/d\theta$) of SL-MCSRM. The mutual-torque (torque produced by mutual-inductance) will contribute to the resultant torque. Hence, SL-MCSRM has the potential to produce higher torque than SL-CSRM. However, in order for the mutual-inductances to contribute positively to the resultant torque, the 3-phase current waveforms need to be properly designed, as will be detailed in the section III.

III. RECTANGULAR CURRENT WAVEFORMS WITH DIFFERENT CONDUCTION ANGLES

A. On-load Torque Expression

The electromagnetic torque of SRMs on the basis of self- and mutual-inductances is given by:

$$T = \overbrace{\frac{1}{2}i_a{}^2\frac{dL_a}{d\theta} + \frac{1}{2}i_b{}^2\frac{dL_b}{d\theta} + \frac{1}{2}i_c{}^2\frac{dL_c}{d\theta}}^{T_{self}}$$
$$\underbrace{+ i_a i_b \frac{dM_{ab}}{d\theta} + i_b i_c \frac{dM_{bc}}{d\theta} + i_a i_c \frac{dM_{ac}}{d\theta}}_{T_{mutual}} \qquad (4)$$

where i_a, i_b and i_c are 3-phase instantaneous currents. It can be seen that the resultant torque can be divided into two components, i.e. self-torque T_{self} and mutual-torque T_{mutual}. Due to the fact that mutual-flux in SL-CSRM is nearly null, its torque component will only comprise of self-torque, i.e. T_{self}. However, the torque component of SL-MCSRM will consist of both T_{self} and T_{mutual} [16].

B. Current Waveforms with Different Conduction Angles

As mentioned previously, not only the self- and mutual-inductances but also the current waveforms will have influence on the electromagnetic torque. Different conduction angles will lead to various performances for different SMRs due to their specific features of self- and mutual-inductances. When SRMs are supplied by rectangular wave current, the value of RMS current is determined by the conduction angle. TABLE II shows the peak current (at 10A RMS current) for conduction angle of 120°, 180°, 240° and 360° elec. which are 17.3A, 14.1A, 12.2A and 10A respectively.

TABLE II. CONDUCTION ANGLE VS PEAK CURRENT

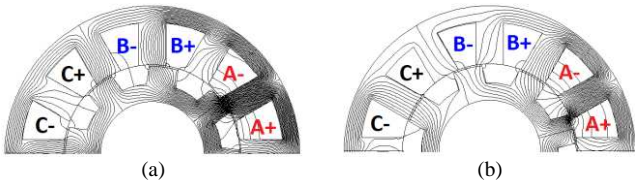| Conduction angle (elec. deg.)	I_{pk}
120	$\sqrt{3}I_{rms}$=17.3A
180	$\sqrt{2}I_{rms}$=14.1A
240	$\sqrt{3/2}I_{rms}$=12.2A
360	I_{rms}=10A

Fig. 5. Rotor positions of SL-MCSRM when $\frac{dM}{d\theta} = 0$, (a) at maximum $|M_{ab}|$, (b) at minimum $|M_{ab}|$. Phase A is supplied by 10A DC current.

Based on the torque equation (4), the self-torque is independent of the sign of the current. It depends only on the sign of $dL/d\theta$. When the rotor poles are approaching the aligned position, $dL/d\theta$ is positive, and hence a positive self-torque is produced, regardless of the sign of the current. In contrast, when the rotor poles are approaching the unaligned position, the self-torque is negative, regardless of the sign of the current as well [22]. Hence, the phase current should be applied when $dL/d\theta$ is positive in order to make sure $\frac{1}{2}i_a{}^2\frac{dL_a}{d\theta}$ is positive. Furthermore, a positive mutual torque relating to two phases, e.g. phases A and B, can be produced when $i_a i_b \frac{dM_{ab}}{d\theta}$ is positive. This requires the i_a and i_b to have the same sign when $\frac{dM_{ab}}{d\theta}$ is positive, or i_a and i_b to have opposite signs when $\frac{dM_{ab}}{d\theta}$ is negative. It can be found that $dM/d\theta$ is positive when the rotor pole approaches the position from Fig. 5 (a) to Fig. 5 (b). Hence, 3-phase currents should be considered together with the

signs of mutual-inductance variations against rotor positions to ensure an optimized positive output torque.
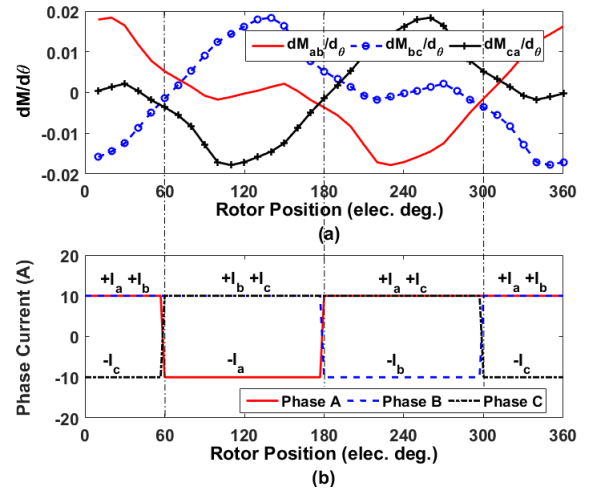

Fig. 6. Derivatives of mutual-inductance with respect to rotor position and relevant current waveform for high mutual-torque generation of SL-MCSRM. (a) $dM/d\theta$ when phases A, B and C are supplied by a 10A dc current, respectively, (b) phase currents (bipolar 360° elec. conduction).

Fig. 6 is an example to analyze the mutual-torque generation of SL-MCSRM. The bipolar 360° elec. is proposed to have a negative 120° elec. conduction and a positive 240° elec. conduction in order to fully utilize the mutual-inductances for torque generation. For example, from rotor position 60° elec. to 180° elec., $dM_{bc}/d\theta$ is positive. Hence, in order to produce a positive mutual-torque between phases B and C, positive i_b and i_c are applied. Additionally, i_a needs to be negative to achieve a positive mutual-torque between phases A and C due to negative $dM_{ac}/d\theta$. The mutual-torque between phases A and B in this region will be negligible regardless the signs of i_a and i_b since $dM_{ab}/d\theta$ is nearly null. Similarly, it can be found that positive mutual-torques are also generated at other rotor positions when supplied by the bipolar 360° elec. conduction shown in Fig. 6 (b).

According to both self- and mutual-inductance variations, rectangular current waveforms have been carried out in Fig. 7, which aims to achieve a balance between the self-torque and the mutual-torque so to maximize the resultant output torque. It is worth noting that Fig. 7 (a) shows a classic 120° elec. conduction, which only produces self-torque. It can be found that the bipolar 180° elec. excitation consists of a negative 60° elec. conduction followed by a positive 120° elec. conduction. The bipolar 240° elec. excitation is comprised of a negative and a positive 120° elec. conduction angles.
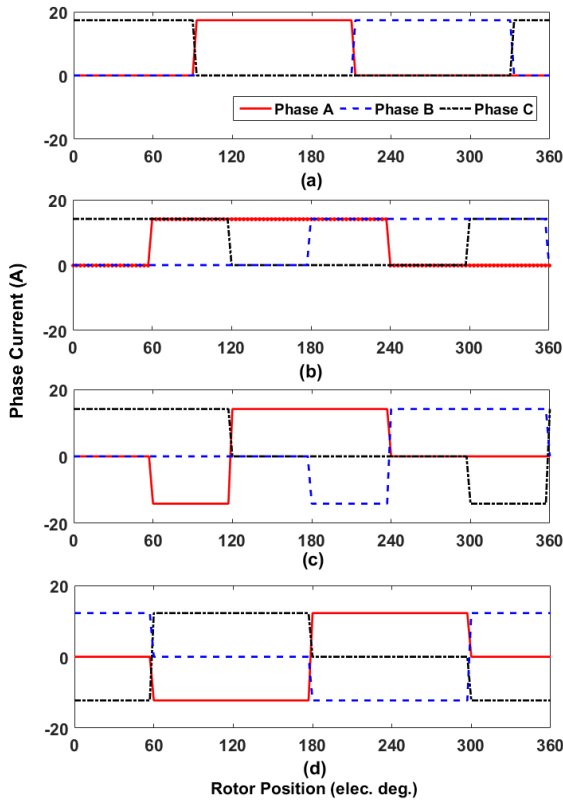
Fig. 7. Unipolar and bipolar excitations with rectangular waveforms and different conduction angles for SL-CSRM and SL-MCSRM. (a) unipolar 120° elec. (b) unipolar 180° elec. (c) bipolar 180° elec. (d) bipolar 240° elec.

For simplicity, these conduction methods can be further expressed as below.

(1). Unipolar $x°$ elec. conduction ($x \leq 180$)

$$
i_A(\theta) = \begin{cases} 0 & 0 \leq \theta < \frac{1}{2}[(\theta_1 + \theta_2) - x] \\ I_{pk} & \frac{1}{2}[(\theta_1 + \theta_2) - x] \leq \theta < \frac{1}{2}[(\theta_1 + \theta_2) + x] \\ 0 & \frac{1}{2}[(\theta_1 + \theta_2) + x] \leq \theta < 360 \end{cases} \quad (5)
$$

(2). Bipolar 180° elec. conduction

$$
i_A(\theta) = \begin{cases} 0 & 0 \leq \theta < \theta_1 \\ -I_{pk} & \theta_1 \leq \theta < \theta_1 + 60 \\ I_{pk} & \theta_1 + 60 \leq \theta < \theta_2 \\ 0 & \theta_2 \leq \theta < 360 \end{cases} \quad (6)
$$

(3). Bipolar 240° elec. conduction

$$
i_A(\theta) = \begin{cases} 0 & 0 \leq \theta < \theta_1 \\ -I_{pk} & \theta_1 \leq \theta < \theta_1 + 120 \\ I_{pk} & \theta_1 + 120 \leq \theta < \theta_2 + 60 \\ 0 & \theta_2 + 60 \leq \theta < 360 \end{cases} \quad (7)
$$

(4). Bipolar 360° elec. conduction

$$
i_A(\theta) = \begin{cases} I_{pk} & 0 \leq \theta < \theta_1 \\ -I_{pk} & \theta_1 \leq \theta < \theta_1 + 120 \\ I_{pk} & \theta_1 + 120 \leq \theta < 360 \end{cases} \quad (8)
$$

The phases B and C will have the same amplitude but out of phase of 120° elec.

IV. PERFORMANCE COMPARISON BETWEEN SRMs WITH DIFFERENT CONDUCTION ANGLES

A. On-load Torque

On-load torques of SL-SRMs have been calculated by 2D-FEM at 10A phase RMS current, as shown in Fig. 8. It

can be found that the on-load torques have different waveforms due to different current waveforms. TABLE III summarizes the comparison of average torque at rated current $10A_{rms}$. The SL-CSRM produces its highest average torque with unipolar 120° elec. conduction. The SL-MCSRM supplied by bipolar 180° elec. conduction achieves its highest average torque.
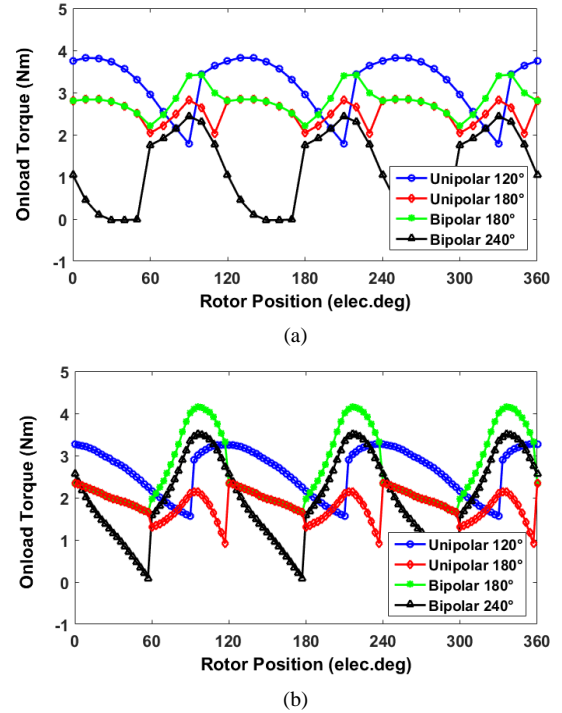

(a)

(b)

Fig. 8. On-load torque comparison of (a) SL-SLCSRM, and (b) SL-MCSRM at 10A phase RMS current.

TABLE III. AVERAGE TORQUE AT RATED CURRENT 10A$_{rms}$

	Rated Average Torque (Nm)	
	SL-CSRM	SL-MCSRM
Unipolar 120° elec.	3.22	2.62
Unipolar 180° elec.	2.82	1.88
Bipolar 180° elec.	2.57	2.65
Bipolar 240° elec.	1.15	2.06

B. Average Torque and Torque Ripple

With different current waveforms in Fig. 7, average torque and torque ripple of the SRMs from 0A to 40A phase RMS current have been investigated, as shown in Fig. 9 and Fig. 10. Torque ripple is calculated according to maximum (T_{max}), minimum (T_{min}) and average torque (T_{av}) for an electrical period as shown below:

$$
T_{ripple} = \frac{T_{max} - T_{min}}{T_{av}} \times 100\% \quad (9)
$$

At low current, SL-CSRM excited by unipolar 120° elec. conduction achieves higher average torque than others as shown in Fig. 9. However, at high current, SL-CSRM supplied by unipolar 180° elec. conduction exhibits better torque capability, i.e. higher average torque while lower torque ripple. According to the nature of self- and mutual-inductance variations, SL-CSRM with bipolar 180°, 240° and 360° elec. conductions have gradually deteriorated performances since negative self-torque has been produced which reduces the average torque (bipolar 360° elec. conduction is not shown here because the average torque is close to zero). For completeness, a DL-CSRM, supplied by unipolar 120° elec. conduction has been selected, which

produces the highest average torque for this class of SRM. It can be found that, with appropriate conduction angle, SL-CSRM can produce higher torque than DL-CSRM at low current. However, due to the fact that SL-CSRM is more sensitive to magnetic saturation, DL-CSRM can produce higher torque at high current.
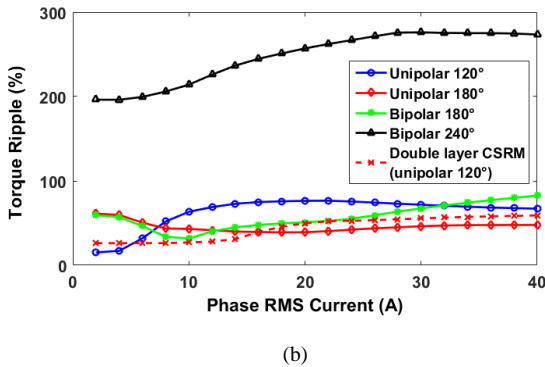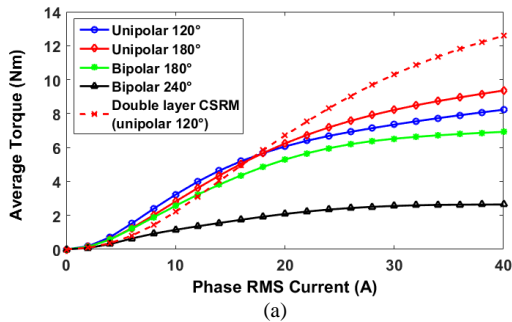

Fig. 9. Comparison of (a) average torque and (b) torque ripple coefficient of SL-CSRM against phase RMS current varying from 0A to 40A.

It can be found in Fig. 10 that SL-MCSRM supplied by bipolar 180° elec. conduction produced highest average torque but modest torque ripple, particularly at high phase current. Compared to DL-MCSRM (which achieved its highest average torque by bipolar 240° elec. conduction if rectangular wave currents are employed), SL-MCSRM with most appropriate conduction angle generated higher torque. However, at high phase current, e.g. 30A, DL-MCSRM produced even higher average torque than that of SL-MCSRM. Moreover, it can be concluded that SL-MCSRM has lower torque ripple than that of DL-MCSRM when supplied with most appropriate conduction angles.
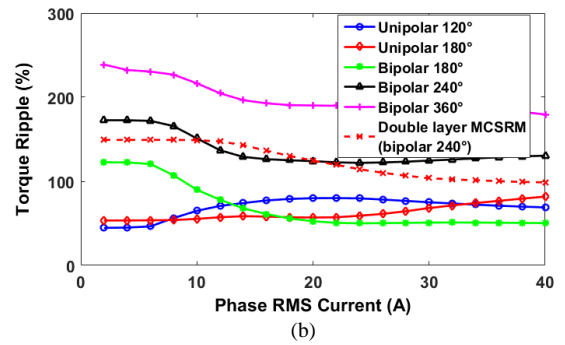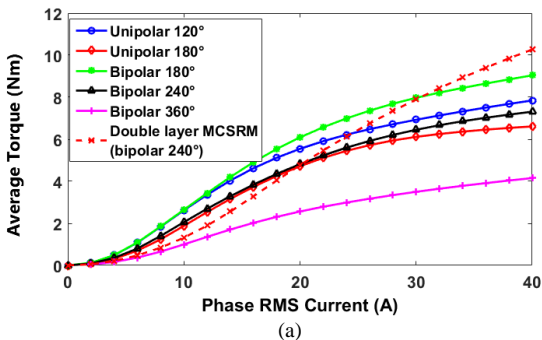

Fig. 10. Comparison of (a) average torque and (b) torque ripple coefficient of SL-MCSRM against phase RMS current varying from 0A to 40A.

C. Copper Loss

Due to SL winding configuration, SL-CSRM and SL-MCSRM have slightly longer end-windings than that of double layer SRMs if the number of turns per phase is the same. Therefore, the phase resistance of SL-CSRM/SL-MCSRM is slightly bigger than that of DL-CSRM/DL-MCSRM. Using the same method in [19], the rated copper losses at 10A phase RMS current for SL and DL-SRMs are calculated as 183W and 153W, respectively. Fig. 11 shows the comparison of average torque and torque ripple against copper loss. It can be found that the copper loss of SL-SRMs is lower than that of double layer SRMs for a given average torque, e.g. 2.5Nm. Moreover, DL-MCSRM has the worst torque against copper loss performance at low copper loss region with the highest torque ripple. However, DL-CSRM supplied by unipolar 120° conduction produces the lowest copper loss at higher average torque, e.g. 8Nm.
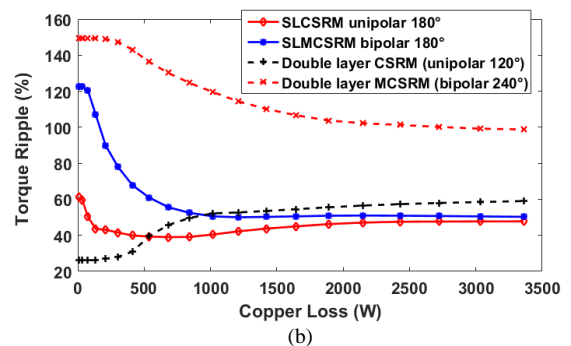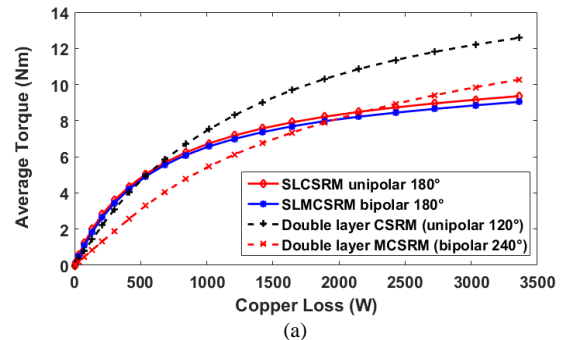

Fig. 11. Comparison of (a) average torque and (b) torque ripple coefficient against copper loss for phase RMS current varying from 0A to 40A.

D. Iron Loss

Due to different excitations, the flux density waveforms in different parts of the machine can be unipolar, asymmetric, and can contain minor-loop excursions. In order to deal with the non-sinusoidal flux waveform, approaches have been proposed in [23] [24]. In this paper, the harmonic flux densities of each FE mesh element of the

stator and rotor have been calculated using Fourier analysis [25] [26], equation (5) is then used for calculating iron loss in each FE mesh element [27]. The total stator and rotor iron losses can be obtained by summing up the losses in all the stator and rotor mesh elements.

$$p_{iron} (W/m^3) = f\left(k_{h1}\Delta B_{pp} + k_{h2}\Delta B_{pp}^2\right) + k_e f \int_0^{1/f} \left(\frac{\partial B}{\partial t}\right)^2 dt \qquad (10)$$

where f is flux density frequency of the stator or rotor, B_{pp} is peak to peak value of flux density. For Silicon iron core considered in this paper, the hysteresis loss coefficients k_{h1} and k_{h2} are $5A/m$ and $40A/m$, respectively. The eddy current loss coefficient k_e is $0.022\ Am/V$.
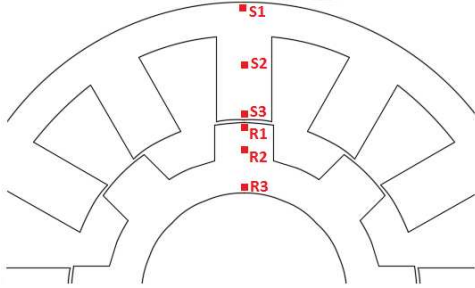

Fig. 12 Cross-section of 12-slot/8-pole SL-SRM. Points S1, S2, and S3 of stator back iron, tooth body, and tooth tip are selected as examples for stator flux density observation. Points R1, R2, and R3 of rotor tooth tip, rotor body and rotor yoke are selected for rotor flux density observation.

In general, iron loss of stator and rotor are calculated separately since their flux densities have different frequencies. Hence, both the radial (B_r) and tangential (B_t) flux densities of stator and rotor are investigated for the selected points shown in Fig. 12. By way of example, one period of flux density variations of stator and rotor tooth bodies of SL-SRMs are shown in Fig. 13 and Fig. 14, respectively. It is found that one period of both the stator B_r and B_t of SL-SRMs is 45 mech. deg., regardless of conduction angles. However, the period of rotor flux densities of SL-CSRM is 120 mech. deg., which is twice as high as that of SL-MCSRM.
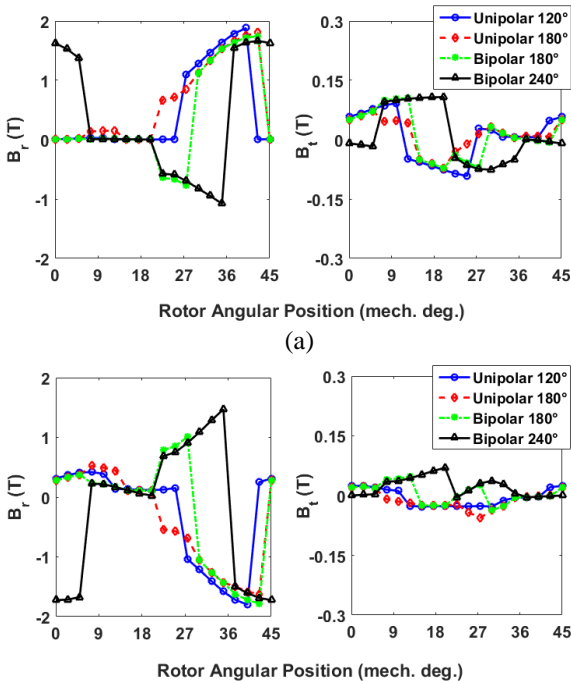

Fig. 13 B_r and B_t vs rotor position at point S2. (a) SL-CSRM, (b) SL-MCSRM. The phase RMS current is 10A for different conduction angles.
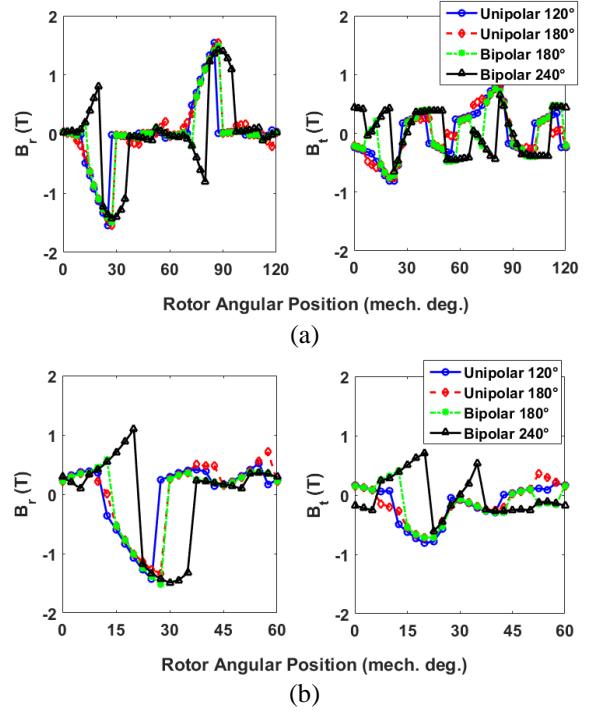

(a)

(b)

Fig. 14 B_r and B_t vs rotor position at point R2. (a) SL-CSRM, (b) SL-MCSRM. The phase RMS current is 10A for different conduction angles.

TABLE IV. SUMMARY OF FLUX DENSITY FREQUENCIES

Machine types	B_r/B_t frequency (Hz)	
	Stator	Rotor
SL-CSRM	f_0	$0.375f_0$
SL-MCSRM	f_0	$0.75f_0$

For simplicity, the stator and rotor flux density frequencies are summarized in TABLE IV. For both SL-CSRM and SL-MCSRM, the stator flux density frequency is equal to $f_0 = \frac{\Omega p}{60}$ (where Ω is mechanical speed and p is rotor pole number), which is 53.33Hz at 400rpm. However, the rotor flux density has lower frequency than the stator. In addition, SL-MCSRM rotor flux density frequency is two times higher than that of SL-CSRM.

TABLE V. IRON LOSS OF SL-SRMS AT $10A_{rms}$, 400RPM

Machine types	Conduction angle (elec. deg.)	Iron loss (W)		
		Stator	Rotor	Total
SL-CSRM	Unipolar 120°	3.58	0.48	4.05
	Unipolar 180°	3.16	0.40	3.57
	Bipolar 180°	4.82	0.60	5.42
	Bipolar 240°	5.90	0.76	6.67
SL-MCSRM	Unipolar 120°	2.33	0.85	3.18
	Unipolar 180°	1.90	0.80	2.71
	Bipolar 180°	3.52	1.13	4.65
	Bipolar 240°	5.03	1.63	6.66

In TABLE V, the stator, rotor and total iron losses have been calculated by 2-D FEM at 10A$_{rms}$ and 400rpm, supplied by rectangular wave current with different conduction angles. It is apparent that both SL-SRMs have higher stator iron losses than rotor iron losses. For completeness, the iron loss variations with increasing phase RMS current at 400rpm are shown in Fig. 15 (a). It is found that both SL-SRMs supplied by conduction angles of

unipolar 120° elec. and unipolar 180° elec. produce lower iron losses than others at different phase RMS currents. With increasing rotor speed at fixed $10A_{rms}$, the iron loss is increased as shown in Fig. 15 (b). It can also be found that the SL-MCSRM produces lower iron loss than SL-CSRM with the same conduction angle at different rotor speeds. At 2000rpm, the highest iron loss is around 60W, which is supplied with conduction angle of bipolar 240° elec. However, the copper loss still could be the dominant loss of this relatively small machine at modest speed. Nevertheless, for larger and higher speed machines, the iron loss could be the dominant loss [28].
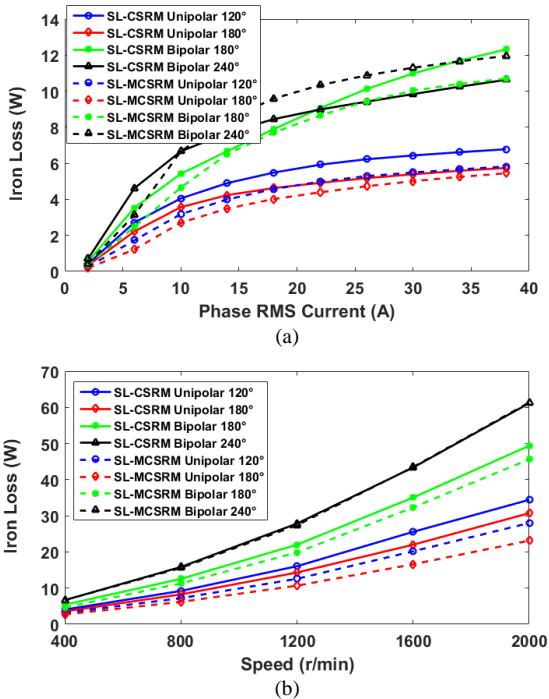

Fig. 15 Influence of conduction angles on iron loss of SL-SRMs. (a) at 400 rpm with increasing phase RMS current, (b) at 10 A_{rms} with increasing speed.

E. Efficiency

The machine efficiency can be calculated based on output power and the previously calculated machine losses. TABLE VI shows the influence of conduction angles on machine efficiency at $10A_{rms}$ under 400rpm rotor speed. Moreover, Fig. 16 shows the efficiency curves with varying rotor speeds at $10A_{rms}$. At 2000rpm, efficiency of > 70% can be achieved for both the SL-SRMs with appropriate current excitations. In addition, with a unipolar 120° elec. conduction angle, the SL-CSRM produces its highest efficiency of 76% at 2000rpm, while SL-MCSRM can achieve 72%. Hence, in order to produce higher efficiency, the appropriate conduction angles of SL-CSRM are unipolar 120° elec. and unipolar 180° elec., whilst for the SL-MCSRM, they are unipolar 120° elec. and bipolar 180°elec.

TABLE VI. EFFICIENCY OF SL-SRMS AT $10A_{rms}$, 400RPM

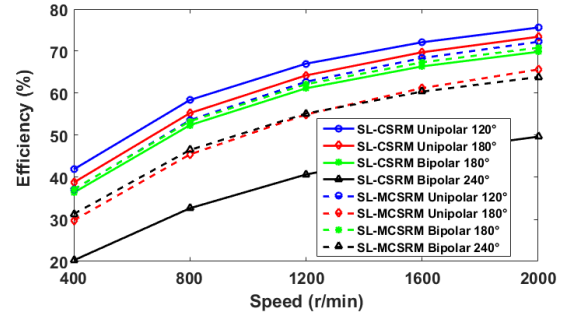| Machine type	Conduction angle (elec. deg.)	Output power (W)	Efficiency (%)
SL-CSRM	Unipolar 120°	134.88	41.90
	Unipolar 180°	118.12	38.77
	Bipolar 180°	107.65	36.36
	Bipolar 240°	48.17	20.25
SL-MCSRM	Unipolar 120°	109.75	37.09
	Unipolar 180°	78.75	29.78
	Bipolar 180°	111.00	37.17

| Bipolar 240° | 86.29 | 31.27 |

Fig. 16 Influence of conduction angles on machine efficiency with varying speed at $10A_{rms}$.

V. EXPERIMENTAL VALIDATION

A. Prototypes of SRMs

In order to validate the predictions, two 12-slot/8-pole machines with the design parameters in TABLE I were built. Fig. 17 (a) is the wound stator of the SL-CSRM and SL-MCSRM. The two SL-SRMs can be realized with the same wound stator by reconnecting the coils as detailed in Fig. 1. The common rotor for both machines is shown in Fig. 17 (b).
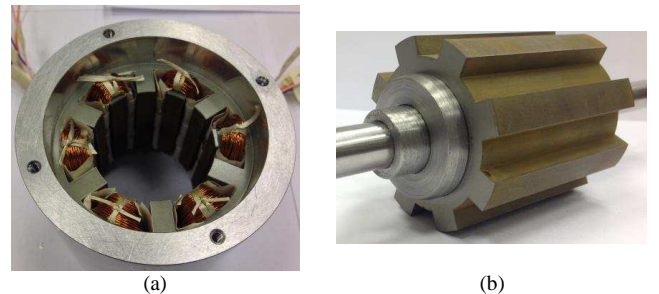

Fig. 17. 12-slot/8-pole prototype SRMs. (a) SL-CSRM or SL-MCSRM stator, (b) 8-pole rotor.

B. Self-and Mutual Inductances

The self-inductance $L_a(\theta)$ and mutual-inductance $M_{ab}(\theta)$ are measured according to (11) and (12) as shown below [29]:

$$L_a(\theta) = \frac{\sqrt{(V_a/I_a)^2 - R_a^2}}{2\pi f} \quad (11)$$

$$M_{ab}(\theta) = \frac{V_b}{2\pi f I_a} \quad (12)$$

where V_a and V_b are the voltages of phase A and phase B, respectively. I_a is the amplitude of phase current in phase A, and f is the frequency of phase voltage. Phase resistance R_a is measured as 1.48Ω for SL-SRMs.

During the tests, the sinusoidal voltage source injected into phase A has a peak-peak value of 9.2V with a frequency of 106.6Hz for SL-CSRM and 105.5Hz for SL-MCSRM. Hence, the measured amplitude of phase current is around 1.8A. Fig. 18 shows the predicted and measured self- and mutual-inductances of SL-SRMs at 1.8A, in which a good agreement can be observed. The discrepancy between measured and predicted self-inductances is mainly

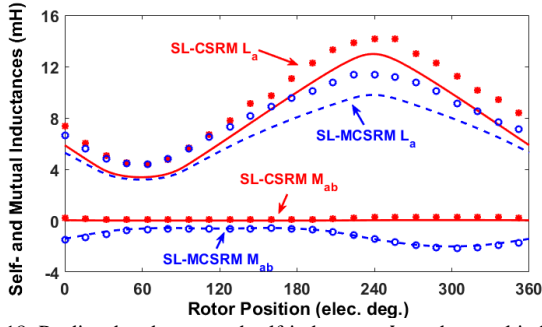due to the end-winding which has not been taken into account in the simulations.

Fig. 18. Predicted and measured self-inductance L_a and mutual inductance M_{ab} at 1.8A phase peak current of SL-SRMs. (solid lines: predicted results, marks: measured results).

C. Self- and Mutual-Torques

In order to measure the torque produced by self-inductance, the phase A is selected as an example. The method of static torque measurement detailed in [30] was adopted for undertaking all torque measurements in this study. Power supply is used to inject DC current of 10A into phase A. Fig. 19 shows the self-torque comparison between SL-CSRM and SL-MCSRM. The measured results are slightly higher than predicted results due to measurement error but this discrepancy is within an acceptable range.

Mutual-torque produced by mutual-inductance is given (8) if the saturation is neglected.

$$T_{ab} = T_{a\&b(series)} - T_a - T_b \qquad (13)$$

where $T_{a\&b(series)}$ is the torque when phase A and phase B are connected in series as shown in Fig. 20, T_a and T_b are self-torque of phase A and phase B, respectively. Fig. 21 shows the comparison of mutual-torque between SL-CSRM and SL-MCSRM, where the phase current of 1A in order to minimize the influence of magnetic saturation. It can be found that the measured results match well with the predictions.
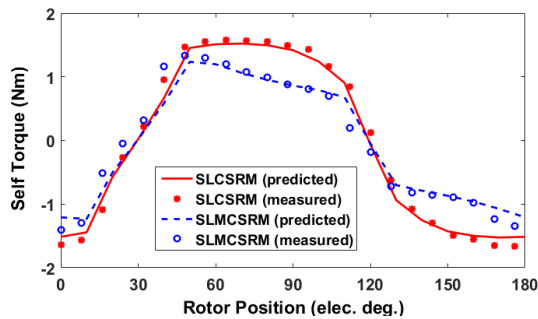

Fig. 19. Predicted and measured self-torques versus rotor position of SL-SRMs at 10A phase DC current.
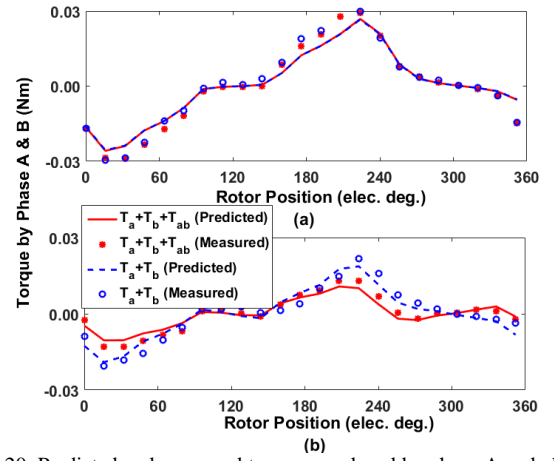

Fig. 20. Predicted and measured torques produced by phase A and phase B versus rotor position at 1A DC phase peak current. (a) SL-CSRM, (b) SL-MCSRM.
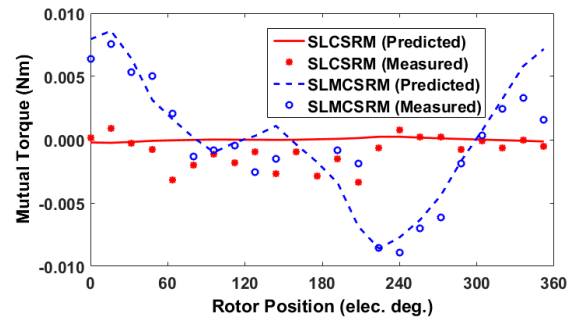

Fig. 21. Predicted and measured mutual-torques versus rotor position at 1A DC phase peak current. (a) SL-CSRM, (b) SL-MCSRM.

D. Static On-load Torque

According to the current waveforms with different conduction angles as shown in Fig. 7, the on-load torques of SL-CSRM and SL-MCSRM have been measured at different rotor positions as shown in Fig. 22. The aligned rotor position of phase A can be tested when phase A is excited. The phase RMS current of all the currents with different conduction angles is 4A, and the dc current is injected into each phase at different rotor positions corresponding to the current waveforms shown in Fig. 7.
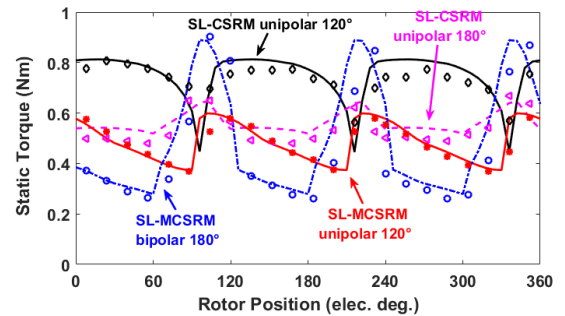
Fig. 22. Predicted and measured static torques versus rotor position at 4A phase RMS current. (Lines: predicted results, marks: measured results).

E. Dynamic test

Limited by the load-torque capacity of the dc machine used for dynamic test, a dc voltage of 38V has been used and the phase RMS current is 4A for all the tests. By way of example, Fig. 23 shows the 3-phase current waveforms of SLCSRM with different conduction angles at 100rpm. The average torque of predicted, static (as shown in Fig. 22) and

dynamic tests at $4A_{rms}$ are compared in **Error! Reference source not found.**.

TABLE VII. AVERAGE TORQUE COMPARSION AT $4A_{rms}$

Machine type	Conduction angle (elec. deg.)	Predicted (Nm)	Static test (Nm)	Dynamic test (Nm)
SL-CSRM	Unipolar 120°	0.75	0.74	0.71
	Unipolar 180°	0.56	0.54	0.55
SL-	Unipolar 120°	0.49	0.48	0.47

MCSRM	Bipolar 180°	0.50	0.47	0.48

The predicted and measured efficiency-speed curves of both the SL-CSRM and SL-MCSRM have been compared in Fig. 24. The measured results have relatively good agreement with the predictions. However, the difference becomes larger at higher speed due to the higher distortion in the transient current waveforms and also the mechanical losses that have not been taken into account in the predictions.
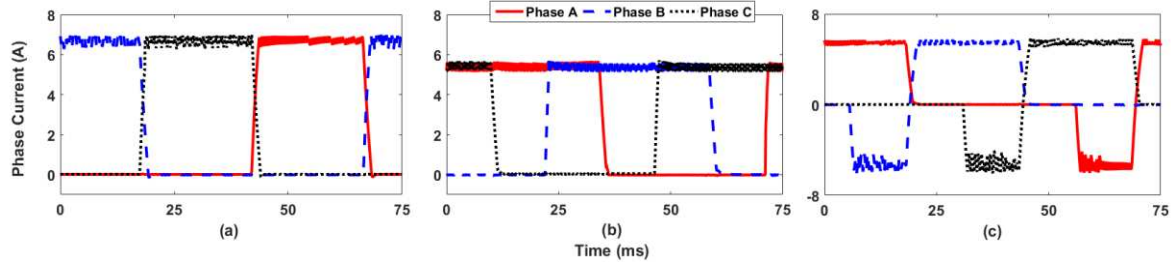

Fig. 23. Transient 3-phase currents with conduction angles of (a) unipolar 120°elec., (b) unipolar 180°elec. and (c) bipolar 180°elec. at 100rpm. The phase RMS current is 4A.
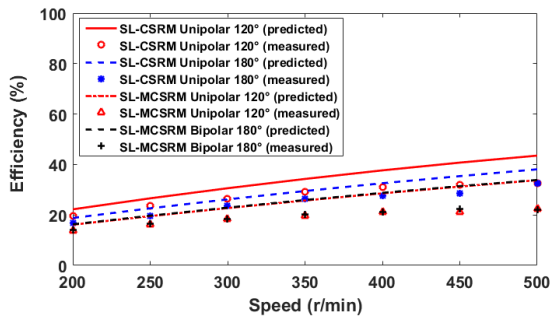

Fig. 24. Predicted and measured efficiency-speed curves of SL-SRMs with different conduction angles. The phase RMS current is 4A.

VI. CONCLUSION

Two single layer, short-pitched SRMs: SL-CSRM and SL-MCSRM supplied by unipolar and bipolar rectangular wave currents with different conduction angles have been investigated and compared in this paper. TABLE VIII summarizes the machine performances with different excitation methods.

TABLE VIII. SUMMARY OF MACHINE AVERAGE TORQUE

	SL-CSRM		SL-MCSRM	
	Low current	High current	Low current	High current
Unipolar 120°	1	2	2	2
Unipolar 180°	2	1	4	4
Bipolar 180°	3	3	1	1
Bipolar 240°	4	4	3	3
Bipolar 360°	5	5	5	5

Note: Number 1-5 represents relative average torque from the highest to the lowest.

Due to the nature of self- and mutual-inductance variations, it is found that SL-CSRM supplied by unipolar 120° conduction obtained its highest average torque at low current. However, at high current, the higher average torque is achieved by unipolar 180° conduction. In addition, SL-CSRM can achieve higher efficiencies when supplied by these conduction angles at different rotor speeds. For SL-MCSRM, bipolar 180° conduction is most appropriate to generate a higher average torque and relative higher efficiency but lower torque ripple than other conduction

angles. When compared to their double layer counterparts, the single layer SRMs have better torque performances at low current. But due to magnetic saturation, double layer SRMs can produce higher average torque at high current.

REFERENCES

[1] A. H. Isfahani and B. Fahimi, "Comparison of mechanical vibration between a double-stator switched reluctance machine and a conventional switched reluctance machine," IEEE Trans. Magn., vol. 50, no. 2, Feb. 26, 2014.

[2] T. J. E. Miller, "Optimal design of switched reluctance motors," IEEE Trans. Ind. Electron., vol. 49, no. 1, pp. 15-27, Feb. 2002.

[3] A. Lebsir, A. Bentounsi, R. Rebbah and S. Belakehal, "Compared applications of permanent magnet and switched reluctance machine: state of the art," in 4th Int. Conf. POWERENG, Istanbul, May 13-17, 2013.

[4] X. B. Liang., G. J. Li, J. Ojeda, M. Gabsi and Z. X. Ren, "Comparative study of classical and mutually coupled switched reluctance motors using multiphysics finite-element modeling," IEEE Trans. Ind. Electron., vol. 61, no. 9, pp. 5066-5074, Oct. 7, 2013.

[5] F. Sahin, H. B. Ertan and K. Leblebicioglu, "Optimum geometry for torque ripple minimization of switched reluctance motors," IEEE Trans. Energy Conver., vol. 15, no. 1, pp. 30-39, Mar. 2000.

[6] G. J. Li, J. Ojeda, S. Hlioui, E. Hoang, M. Lecrivain and M. Gabsi, "Modification in rotor pole geometry of mutually coupled switched reluctance machine for torque ripple mitigating," IEEE Trans. Magn., vol. 48, no. 6, pp. 2025-2034, Dec. 9, 2011.

[7] P. C. Desai, M. Krishnamurthy, N. Schofield and A. Emadi, "Novel switched reluctance machine configuration with higher number of rotor pole than stator poles: concept to implementation," IEEE Trans. Ind. Elec., vol. 57, no. 2, pp. 649-659, Oct. 20, 2009.

[8] R. Mikail, I. Husain, Y. Sozer, M. S. Islam and T. Sebastian, "Torque-ripple minimization of switched reluctance machines through current profiling," IEEE Trans. Ind. Appl., vol. 49, no. 3, pp. 1258-1267, Mar. 13, 2013.

[9] R. Mikail, I. Husain, M. S. Islam, Y. Sozer and T. Sebastian, "Four-quadrant torque ripple minimization of switched reluctance machine through current profiling with mitigation of rotor eccentricity problem and sensor errors," IEEE Trans. Ind. Appl., vol. 51, no. 3, pp. 2097-2104, May 15, 2015.

[10] X. Liu, Z. Q. Zhu, M. Hasegawa, A. Pride and R. Deodhar, "Investigation of PWMs on vibration and noise in SRM with sinusoidal bipolar excitation," in 21st IEEE-ISIE, Hangzhou, China, May 28- 31, 2012.

[11] J. W. Ahn, S. G. Oh, J. W. Moon and Y. M. Hwang, "A three-phase switched reluctance motor with two-phase excitation," IEEE Trans. Ind. Appl., vol. 35, no. 5, pp. 1067-1075, Sep./Oct. 1999.

[12] J. Ahn, S. Oh, J. Moon and Y. Hwang, "A three-phase switched

reluctance motor with two-phase excitation," IEEE Trans. Ind. Appl., vol. 35, no. 5, pp. 1067-1075, 1999.

[13] J. W. Ahn, S. J. Park and D. H. Lee, "Hybrid excitation of SRM for reduction of vibration and acoustic noise," IEEE Trans. Ind. Electron, vol. 51, no. 2, pp. 374-380, April 2004.

[14] X. Liu, Z. Q. Zhu, M. Hasegawa, A. Pride, R. Deohar, T. Maruyama and Z. Q. Chen, "Performance comparison between unipolar and bipolar excitations in switched reluctance machine with sinusoidal and rectangular waveforms," in Energy Conversion Congress and Exposition (ECCE), Phoenix, AZ, Sept. 17-22, 2011.

[15] G. J. Li, Z. Q. Zhu, X. Y. Ma and G. W. Jewell, "Comparative study of torque production in conventional and mutually coupled SRMs using frozen permeability," IEEE Trans. Magn., no. 9, Jan. 12, 2016.

[16] X. Y. Ma, G. J. Li, G. Jewell and Z. Q. Zhu, "Comparative study of short-pitched and fully-pitched SRMs supplied by sine wave currents," in ICIT15, Sevilla, Spain, Mar. 17-19, 2015.

[17] B. C. Mecrow, "Fully pitched-winding switched reluctance and stepping-motor arrangements," IET Elec. Power Appl., vol. 40, no. 1, pp. 61-70, Jan. 1993.

[18] B. C. Mecrow, "New winding configurations for doubly salient reluctance machines," IEEE Trans. Ind. Appl., vol. 32, no. 6, pp. 1348-1356, Dec. 1996.

[19] X. Y. Ma, G. J. Li, G. W. Jewell, Z. Q. Zhu and H. L. Zhan, "Performance comparison of doubly salient reluctance machine topologies supplied by sinewave currents," IEEE Trans. Ind. Electron., (in press).

[20] W. Hua, H. Hua, N. Dai, G. S. Zhao and M. Cheng, "Comparative study of switched reluctance machines with half-and full-teeth-wound windings," IEEE Trans. Ind. Electron., vol. 63, no. 3, pp. 1414-1424, Feb. 3, 2016.

[21] D. A. Staton, R. P. Deodhar, W. L. Soong and T. J. E. Miller, "Torque prediction using the flux-MMF diagram in AC, DC, and reluctance motors," IEEE Trans. Ind. Appl., vol. 32, no. 1, pp. 180-188, Jan. 1996.

[22] T. J. E. Miller, Brushless permanent-magnet and reluctance motor drives, New York: Oxford university press, 1989.

[23] Y. Hayashi and T. J. E. Miller, "A new approach to calculating core losses in the SRM," IEEE Trans. Ind. Appl., vol. 31, no. 5, pp. 1039-1046, Sep./Oct. 1995.

[24] J. D. Lavers, P. P. .. Biringer and H. Hollitscher, "A simple method of estimating the minor loop hysteresis loss in thin laminations," IEEE Trans. Magn., vol. 14, no. 5, pp. 386-388, Sep. 1978.

[25] P. N. Materu and R. Krishnan, "Estimation of switched reluctance motor losses," IEEE Trans. Ind. Appl., vol. 28, no. 3, pp. 668-679, May/June 1992.

[26] J. F. Liu, X. b. Zhang, H. J. Wang and J. F. Bao, "Iron loss characteristic for the novel bearingless switched reluctance motor," in ICEM, Busan, Korea, Oct. 26-29, 2013.

[27] G. J. Li, J. Ojeda, E. Hoang, M. Lecrivain and M. Gabsi, "Comparative studies between classical and mutually coupled switched reluctance motors using thermal-electromagnetic analysis for driving cycles," IEEE Trans. Magn., vol. 47, no. 4, pp. 839-847, Apr. 2011.

[28] S. D. Calverley, G. W. Jewell and R. J. Saunders, "Prediction and measurement of core losses in a high-speed switched-reluctance machine," IEEE Trans. Magn., vol. 41, no. 11, pp. 4288-4298, Nov. 2005.

[29] G. J. Li, Z. Q. Zhu, W. Q. Chu, M. P. Foster and D. A. Stone, "Influence of flux gaps on electromagnetic performance of novel modular PM machines," IEEE Trans. Energy Convers., vol. 29, no. 3, pp. 716-726, Sep. 2014.

[30] Z. Q. Zhu, "A simple method for measuring cogging torque in permanent magnet machines," in IEEE Power & Energy Society General Meeting,, Jul. 26-30, 2009.